Comparison of Walking and Traveling-Wave Piezoelectric Motors as Actuators in Kinesthetic Haptic Devices

Pontus Olsson, Fredrik Nysjö, Ingrid B. Carlbom, and Stefan Johansson

Abstract—Piezoelectric motors offer an attractive alternative to electromagnetic actuators in portable haptic interfaces: they are compact, have a high force-to-volume ratio, and can operate with limited or no gearing. However, the choice of a piezoelectric motor type is not obvious due to differences in performance characteristics. We present our evaluation of two commercial, operationally different, piezoelectric motors acting as actuators in two kinesthetic haptic grippers, a walking quasi-static motor and a traveling wave ultrasonic motor. We evaluate each gripper's ability to display common virtual objects including springs, dampers, and rigid walls, and conclude that the walking quasi-static motor is superior at low velocities. However, for applications where high velocity is required, traveling wave ultrasonic motors are a better option.

Index Terms—Piezoelectric, walking motor, traveling-wave motor, actuator, haptic gripper

1 Introduction and Related Work

THE choice of actuators is important in high-fidelity haptic interfaces. Desired properties include large force and velocity ranges, fast response time, and no backlash. Torque/volume and torque/mass ratios are also important, especially when the hand carries the weight of the device.

Piezoelectric motors, in contrast to electromagnetic (EM) motors which are presently the most common actuator in kinesthetic haptic displays, offer higher force-to-volume and force-to-mass ratio at the motor shaft without gearbox [1], a desirable property for integration into haptic interfaces [2]. Their operational velocity is generally much lower than EM motors while their maximum continuous force/torque is higher, which allows direct-drive without reduction gearing and backlash. When the motor is not actively driven, the shaft is firmly held by friction forces which make piezoelectric motors particularly suitable for haptic display of high impedances such as stiff virtual walls. Another advantage is the possibility to build non-magnetic motors compatible with medical magnetic resonance imaging (MRI) environments [3].

We compare the performance of two commercial piezoelectric motors, a rotational traveling wave ultrasonic motor (TWUM) and a linear walking quasi-static motor (WQSM), integrated in two kinesthetic haptic grippers. We chose motors that produce the same order of force magnitude at the user's point of contact. However, the inherent differences of the motors, for example linear vs. rotational, mean that the devices require different design strategies. This study should provide guidance in choosing the best motor type for a given application.

Albeit rare compared to EM motors, the TWUM is the most common piezoelectric motor in haptics research. Examples include non-magnetic devices compatible with MRI-scanners [4] and TWUM-specific force-feedback control [5]. WQSM's for haptics are even more rare [2] but, as we shall see, offer advantages for some applications. The inherent characteristics of the actuators presented here are representative of the piezoelectric actuator families to which they belong.

TWUMs operate at ultrasonic frequencies close to mechanical resonance, above the limit of human hearing [6]. Two phase-shifted sinusoidal drive signals induce a traveling flexural wave in a ring-shaped stator; see Fig. 1A. The wave motion drives by friction a rotor (B), which is preloaded by a strong spring (C) against the stator. The rotational direction of the motor is determined by the phase shift between the drive signals. Compared to quasi-static motors, TWUMs' higher drive frequencies generally enable a higher maximum velocity.

Fig. 1 (bottom) shows the principle of a linear WQSM. These motors operate in an audible frequency range well below resonance, hence quasi-static. The active parts in a WQSM stator are piezoelectric legs that can be elongated and bent making it possible to "walk" a drive rod by driving the legs in two pairs, 180° out of phase. The positional precision is extremely high with fractional steps as short as a single nanometer [7], and the non-resonant operation offers a high max/min velocity ratio, limited only by the driving electronics.

2 Gripper Designs

We compare the performance of the two motors integrated in two prototype kinesthetic haptic grippers; see Fig. 2. Tables 1 and 2 summarize gripper and motor specifications, respectively. For comparison we included in Table 2a Maxon 118754 RE-25 EM motor used in the "Haptic Paddle" device described in [8].

The WQSM gripper (Fig. 2 top) is actuated by a linear WQSM (A), a Piezo LEGS LT2010 from PiezoMotor [7], that drives the index finger part (F) along an arc path, guided by eight ball bearings mounted tightly against a curved rail on the finger part. The selected leverage magnifies the motor speed about four-and-a-half times at the index finger thimble, resulting in a maximum speed of 70 mm/s with an index finger part length of 70 mm, while the maximum force is reduced with the same factor. For more details we refer the reader to [2]. The TWUM gripper (Fig. 2 bottom) is actuated by two rotational TWUMs (K, L), PUMR40E from Piezotech [9], whose motor axes attach rigidly to two finger parts; one for the thumb thimble (M) and one for the remaining fingers (N). Both grippers have high resolution position encoders (G in the WQSM gripper, and integrated in the TWUM housing), and strain gauge force/torque sensors (J, P).

2.1 Motor Drive Modes

The motor-specific drivers map a drive command, V_c, in the range −1 to 1, to motor-specific drive parameters; see Fig. 3. The sign and amplitude of V_c dictate motor direction and velocity, respectively. Both motors exhibit a nearly linear velocity reduction with external load.

The conventional TWUM drive is frequency drive (FD), with a drive frequency, f_{drive}, and a phase shift, ϕ_{drive} between the motor's two sinusoidal driving voltages whose sign dictates motor direction. The motor operates close to its resonance frequency, f_r, and the velocity and torque is controlled by adjusting the drive frequency f_{drive}. However, FD suffers from a non-linear velocity deadband unsuitable for haptics, typically around 10 percent of maximum velocity [4].

Instead, we drive the motor in bursts, as discussed in [10]. This mode, here denoted pulse-train drive (PTD), fixes the drive frequency at 36.8 kHz, close to resonance, and switches the continuous close-to-resonance signals on/off with an adjustable duty cycle at a fixed, audible frequency (500 Hz). A lower switching frequency would allow higher duty cycle resolution as more clock cycles pass between each switch, but would fall within the limits

- *P. Olsson, F. Nysjö, and I.B. Carlbom are with the Department of Information Technology, Uppsala University, Uppsala, Sweden. E-mail: {pontus.olsson, fredrik.nysjo, ingrid.carlbom}@it.uu.se.*
- *S. Johansson is with the Department of Engineering Sciences, Uppsala University, Uppsala, Sweden. E-mail: stefan.johansson@angstrom.uu.se.*

Manuscript received 28 Aug. 2015; revised 29 Dec. 2015; accepted 4 Jan. 2016. Date of publication 30 Mar. 2016; date of current version 14 Sept. 2016.
Recommended for acceptance by F. Giraud.
For information on obtaining reprints of this article, please send e-mail to: reprints@ieee.org, and reference the Digital Object Identifier below.
Digital Object Identifier no. 10.1109/TOH.2016.2537803

1939-1412 © 2016 IEEE. Translations and content mining are permitted for academic research only. Personal use is also permitted, but republication/redistribution requires IEEE permission. See http://www.ieee.org/publications_standards/publications/rights/index.html for more information.

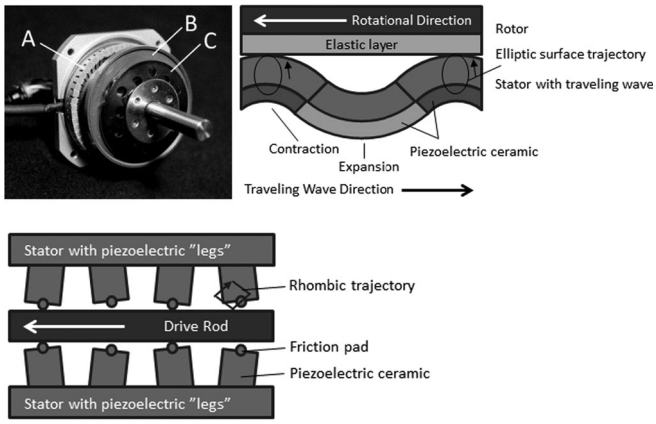

Fig. 1. Key components of a TWUM (top left): Stator with teeth (A); rotor (B); and pre-load spring (C). TWUM principle (top right): Expansion and contraction of piezoelectric elements in the stator induces a traveling wave that generates torque in the rotor by friction contact. WQSM principle (bottom): The piezoelectric legs "walk" the drive rod. The motion amplitudes are exaggerated.

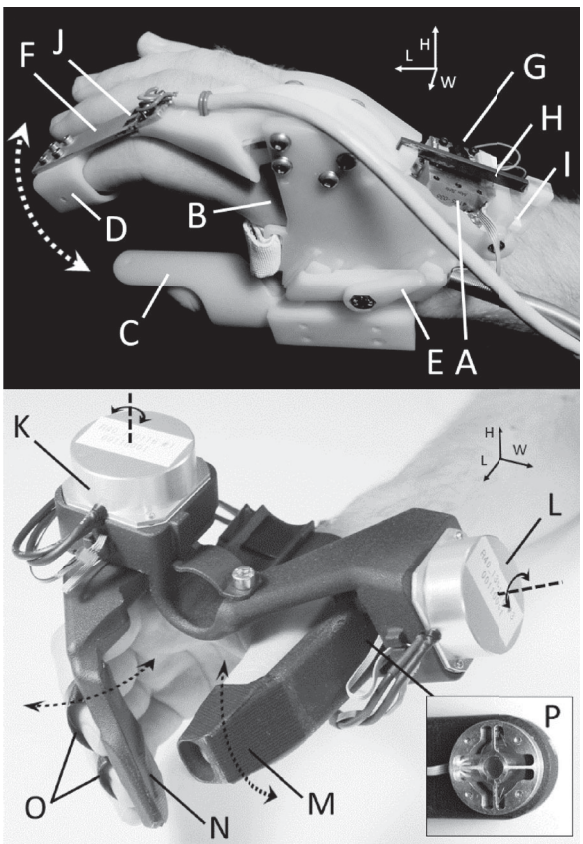

Fig. 2. WQSM gripper (top): Piezo LEGS LT2010 (A); rotational point (B); thumb tube (C); index finger thimble (D); size adjustment screw (E); index finger part (F); magnetic position encoder (G); magnetic rod (H); motor drive rod (I); strain gauge sensor (J). TWUM gripper (bottom): PUMR40E (K, L); thumb thimble (M); finger plate (N); finger straps (O); and torque sensor (P). Dashed arrows indicate finger part motions.

for human vibrotactile sensing [11]. Increasing the PTD switching frequency shortens the "on-time" in each PTD cycle at a given PTD percentage, which may prevent the stator from reaching operational resonance conditions. The goal is to increase the force at low drive commands, to allow lower velocities. The TWUM driver linearly maps the absolute value of V_c to a duty cycle percentage of the pulse-train switching function, and the sign of V_c determines the sign of ϕ_{drive}. The special case $\phi_{drive} = 0$ generates no motion, but lowers the friction between the rotor and the stator significantly if f_{drive} is close to f_r, which can be used to display free motion [12].

TABLE 1
Gripper Specifications. Forces, and Velocities Assume Finger Part Lengths of 70 mm

Gripper Type	WQSM Gripper	TWUM Gripper
Size (LxWxH)	155 × 28 × 85 mm	125 × 145 × 85 mm
Force Range	± ~5 N	± ~2 N
Velocity Range	± ~70 mm/s	± ~900 mm/s
Motion Range	45 mm (Index finger)	60 mm (Thumb) 65 mm (Other)
Weight	130 g	400 g

TABLE 2
Motor Specifications

Motor Type	WQSM (LT2010)	TWUM (PUMR40E)	Maxon 118754
Length	22 mm	44 mm	54.5 mm
Width	11 mm	44 mm	25 mm
Height	21 mm	18.5 (35.5) mm	25 mm
Hold. Force	22 N	0.2 Nm	N/A
Max Force	20 N	0.15 Nm	0.28 Nm
Cont. Force	20 N	0.15 Nm	0.027 Nm
Max Velocity	±15 mm/s	80 rpm	11,000 rpm
Weight	29 g	90 g (110 g)	130 g

Parentheses Indicate Size Measurements Including Angular Encoder.

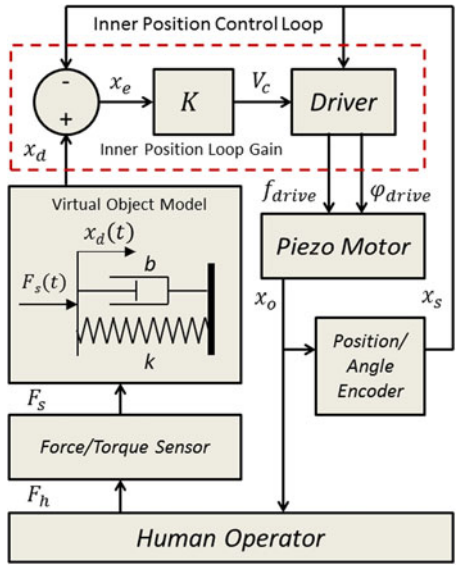

Fig. 3. Gripper system schematics.

A WQSM has no dead-band and can be controlled directly by f_{drive} which is held within a sub-resonance span, in our case between 33 and 2.5 kHz. Higher frequencies may damage the motor. Typically, the zero-load motor velocity increases linearly with drive frequency [7]. The WQSM driver linearly maps the absolute value of V_c to f_{drive} such that the defined frequency span can be fully reached within the span of V_c. The sign of V_c sets the phase shift ϕ_{drive} between the motors two drive signals to $\pm 90°$ for forward or backwards direction.

For $f_{drive} = 0$, both motors "lock" up to a maximum holding force, which we use to display rigid walls. If loads exceed the holding force, the shaft slips with negligible wear [7].

2.2 System Architecture and Control

Fig. 3 shows the grippers' control system architecture, based on a classical admittance scheme with an inner control loop, commonly employed in robotics [13]. WQSMs and TWUMs are non-back-drivable since the rod/rotor is always in friction contact with the

TABLE 3
Stall Forces and Zero-Load Velocities for the WQSM and TWUM Grippers at Six Different Values of V_c

V_c	Stall Force (N)		Zero-Load Vel. (mm/s)	
	WQSM	TWUM	WQSM	TWUM
0.02	**4.1** (0.03)	**0.0** (0.00)	**0.9** (0.1)	**0.0** (0.0)
0.05	**4.1** (0.03)	**0.4** (0.01)	**3.8** (0.1)	**4.8** (1.6)
0.1	**4.2** (0.02)	**1.0** (0.00)	**8.0** (0.1)	**31.9** (4.1)
0.2	**4.4** (0.05)	**1.5** (0.01)	**15.8** (0.3)	**182.3** (24.3)
0.5	**5.3** (0.03)	**2.0** (0.02)	**39.2** (0.6)	**575.5** (74.4)
1.0	**5.6** (0.03)	**2.2** (0.02)	**69.8** (1.8)	**929.0** (111.1)

Parentheses indicate standard deviations.

stator, and thus well-suited for admittance control. A force sensor samples the human force F_h. The sampled force F_s drives a virtual object model with an admittance parametrized by a stiffness of k N/mm and a damping of b Ns/mm. The dynamic behavior of the model can be described as a first order differential equation relating position, velocity, and applied force: $kx_d(t) + b\,x_d^{(t)} = F_s(t)$. The model's positional state x_d serves as a desired position to an inner high-gain positional control loop (within the dashed box), that drives the motor towards x_d. An encoder samples the motor position x_o, and the sampled position x_s is fed back to the inner position loop. The system runs at a fixed rate of 150 Hz.

3 Evaluation and Analysis

Many factors contribute to the overall performance of a haptic device, including physical design, sensors, actuation, and control strategy. Here we focus on the differences in performance resulting from the choice of piezoelectric motor type for actuation. For the TWUM gripper, we only include the results for the thumb thimble. We sample all data at 150 Hz.

3.1 Force and Velocity Evaluation

To evaluate stall force (load at which the motor velocity goes to zero), we drive the grippers' finger parts against a rigid stop with a series of drive commands of logarithmically increasing magnitude. We repeat each drive command four times and record the force sensor readings during one second after reaching steady state. To evaluate zero-load velocity, we let the finger parts of the grippers move freely, and execute the same series of drive commands. We estimate velocities by differentiation of sampled positions, x_s. Table 3 shows the stall force and zero-velocity means with standard deviations within parentheses. The results assume finger part lengths of 70 mm for both grippers.

The WQSM provides substantial stall force over the whole drive parameter span, in contrast to the pulse-train driven TWUM which falls below 50 percent of max force in the lowest 10 percent of the span. The sections of the drive parameter spans yielding stall forces exceeding 1 N correspond to a min/max velocity ratio of approximately 1:30 for the TWUM. The minimum velocity of the WQSM is in our case a lower frequency limit on the drive electronics at 33 Hz. In contrast to TWUMs, WQSMs can generally operate at arbitrarily low frequencies and thus velocities.

3.2 Admittance Fidelity Evaluation

The device's displayed admittance should match the admittance of the simulated virtual object with minimal distortion. We test the two grippers' admittance fidelity in a test rig while simulating and displaying simple virtual objects: springs, dampers, and rigid walls, common basic building blocks in virtual environments. The test rig uses a servo-motor to displace two antagonistic, stretched extension springs in a sinusoidal, longitudinal motion with peak-to-peak amplitude of 50 mm. By attaching a finger part (the index finger thimble for the WQSM gripper and the thumb thimble for the TWUM gripper) of a gripper to the equilibrium point between the springs, the springs become a sinusoidal force source if the gripper displays a rigid virtual wall and a sinusoidal position source if the gripper displays free motion. The antagonistic springs exhibit an effective stiffness of 0.38 N/mm at the gripper connection point. For each gripper in the test rig we set the inner position loop gain to the highest possible value before losing stability.

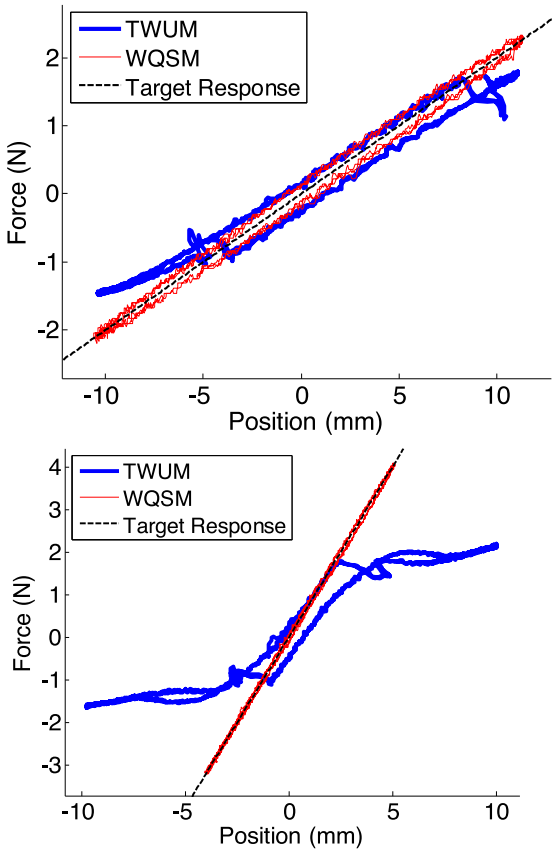

Fig. 4. Virtual spring with target stiffness k = 0.2 N/mm (top) and 0.8 N/mm (bottom).

Many applications require a wide span in stiffness and damping. We probe a large number of stiffness and damping parameters at various test rig rates. Below we give examples of parameter value combinations at which display errors clearly expose differences in the grippers' performance. We sample forces and positions from the grippers during repeated test cycles and compare with the target forces and positions shown as dashed lines in Figs. 4, 5, and 6. Table 4 shows root mean square error (RMSE) between measured and target forces for the virtual springs and dampers in newtons and as a percentage of the maximum gripper forces.

3.2.1 Virtual Spring and Damper

We render two virtual springs, one soft with stiffness k = 0.2 N/mm and one stiffer with k = 0.8 N/mm, and apply a repeated, sinusoidal motion with the test rig at a low rate, 0.125 Hz. Some damping is required for stability, so we simulate all springs with a low damping of 0.015 Ns/mm. Fig. 4 shows force vs. position for the soft (top) and stiff (bottom) springs. We attribute the TWUM force spikes to the TWUM's limitation at low velocities. In addition, it reaches its upper force limit around 2 N. The WQSM has no dead-band, which combined with its higher maximum force explains this gripper's superior virtual spring tracking results at both stiffness levels.

Displaying low damping is often a challenge with admittance devices. We render a virtual damper with low damping, b = 0.020 Ns/mm, and zero spring stiffness and apply a repeated,

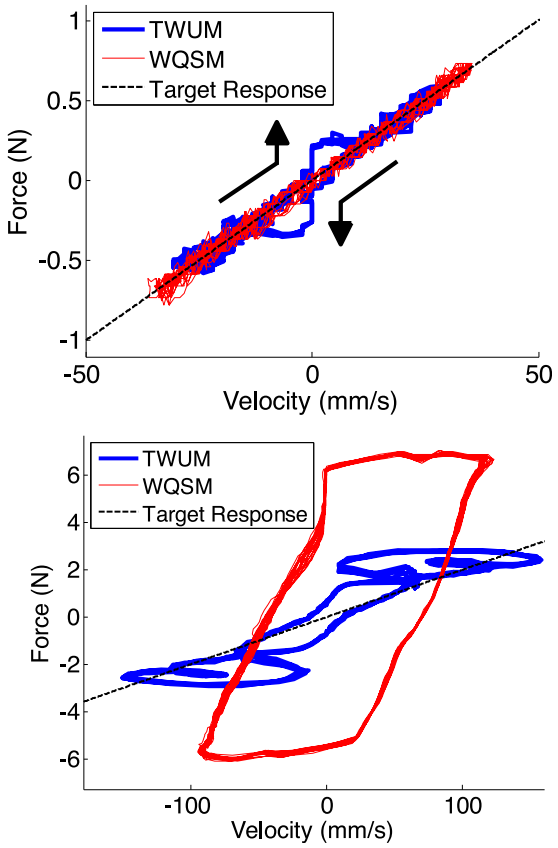

Fig. 5. Virtual damper with target b = 0.02 Ns/mm. Test rig rate 0.25 Hz (top) and 1.0 Hz (bottom).

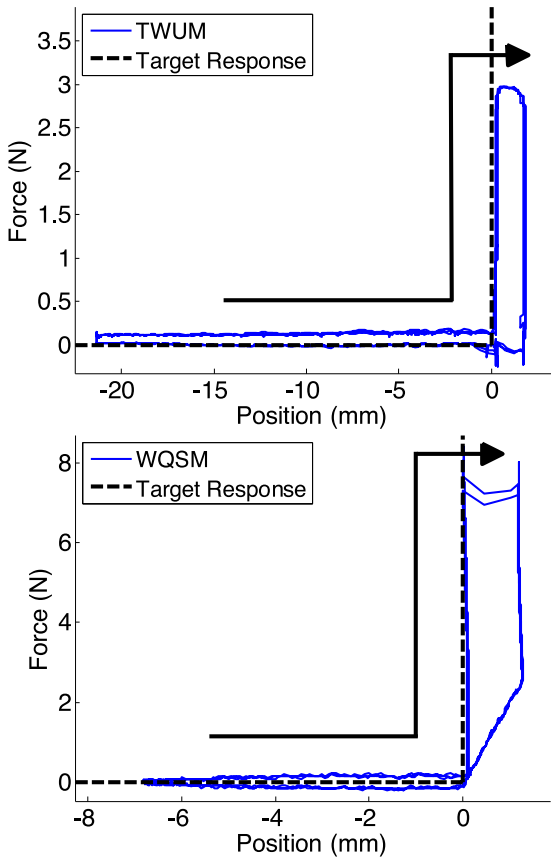

Fig. 6. Virtual wall. TWUM gripper (top) and WQSM gripper (bottom). Note the different scales.

TABLE 4
RMSE for the Virtual Springs and Dampers in Newtons (N) and as a Percentage of the Maximum Gripper Forces, 2 and 5 N for the TWUM and WQSM, Respectively

Virtual Object	TWUM Gripper	WQSM Gripper
Spring 0.2 N/mm	0.377 N (18.9%)	0.112 N (2.2%)
Spring 0.8 N/mm	3.835 N (191.8%)	0.072 N (1.4%)
Damper 0.25 Hz	0.060 N (3%)	0.036 N (0.7%)
Damper 1.0 Hz	0.703 N (35.2%)	3.497 N (69.9%)

sinusoidal motion with the test rig at a slow rate, 0.25 Hz, and a faster rate, 1.0 Hz.

Fig. 5 shows force vs. velocity for the slow (top) and fast (bottom) oscillations, respectively. Note the zero-velocity force spikes for the TWUM gripper, which we again explain by the difficulty of driving the motor at the lowest velocities. For the fast oscillations, the maximum force is reached between 1.5 and 2 N, leading to a transient oscillation, however within the provided force span the gripper behaves smoothly. The WQSM gripper, lacking the dead-band, shows the most accurate tracking for slow oscillations. For fast oscillations, the highest test rig velocity exceeds the maximum motor velocity of 70 mm/s which causes large deviations from the target response.

3.2.2 *Virtual Wall and Free Motion*

To simulate slow gripping of a rigid object, we render a virtual rigid wall by simply turning off the motor when in contact with the wall (at position $x = 0$), and apply a repeated, 0.125 Hz, sinusoidal motion with the test rig.

When $x < 0$, the gripper is in "free motion". For the WQSM gripper, we achieve free motion by simulating low damping, 0.015 Ns/mm. Stable display of zero damping is unfortunately not possible under admittance control, as zero damping implies infinite admittance. For the TWUM, instead of low damping, we set $\varphi_{drive} = 0$ to display free motion.

Fig. 6 shows force versus position for the TWUM (top) and the WQSM (bottom) grippers. The TWUM gripper presents a stiff response against the wall up to its holding force, between 2.5 and 3 N, where it slips through the wall. The holding force presents a distinct difference to the low 0.2 N resistance force we obtain from the low friction mode. The WQSM gripper also presents a stiff response against the wall up to its holding force around 7 N.

4 Discussion and Conclusion

The WQSM is superior for applications where accurate tracking and very stiff feedback at low velocities is desired, such as fine manipulation tasks where force spikes around zero velocity could be very disturbing to users. Its velocity and position are very straightforward to control with frequency drive, and it provides the rated maximum stall force over the whole drive frequency span. The WQSM also provides higher force than the TWUM, and is smaller and lighter. However, the WQSM needs leverage in our gripper to reach desired maximum velocities, which requires careful design, and its limited maximum velocity severely limits its performance at higher velocities. Users may perceive this too restraining in high-velocity applications such as game controllers. Here ultrasonic motors such as a TWUM are a better option. The pulse train drive gives a larger velocity span than the conventional frequency drive at the expense of audible noise. TWUMs also provide a "low friction" mode for the display of free motion.

Acknowledgments

The Knowledge and Vårdal Foundations, VINNOVA, SSF, and ISA supported this research.

REFERENCES

[1] M. Bexell, and S. Johansson, "Fabrication and evaluation of a piezoelectric miniature motor," *Sens. Actuators A, Phys.*, vol. 75, no. 1, pp. 8–16, 1999.

[2] P. Olsson, S. Johansson, F. Nysjö, and I. B. Carlbom, "Rendering stiffness with a prototype haptic glove actuated by an integrated piezoelectric motor," in *Proc. Eurohaptics*, Tampere, Finland, 2012, pp. 361–372.

[3] M. Flueckiger, M. Bullo, D. Chapuis, R. Gassert, and Y. Perriard, "fMRI compatible haptic interface actuated with traveling wave ultrasonic motor," in *Proc. Industry Appl. Conf.*, 2005, vol. 3, pp. 2075–2082.

[4] C. Parthiban, C. Esser, and M. R. Zinn, "Evaluation of a parallel actuation approach for MR-compatible haptics," in *Proc. IEEE Haptics Symp.*, 2012, pp. 563–570.

[5] T. M. Seigler, N. Venkatesan, and D. Inman, "An approach to force-feedback control with traveling wave ultrasonic motor," *J. Intell. Mater. Syst. Struct.*, vol. 20, no. 12, pp. 1393–1400, 2009.

[6] T. Sashida, and T. Kenjo, *Introduction to Ultrasonic Motors*. Oxford, U.K.: Clarendon, 1993.

[7] (2016, Apr.) [Online]. Available: http://www.piezomotor.com/

[8] B. Hannaford and A. M. Okamura, "Haptics," *Springer Handbook of Robotics*, New York, NY, USA: Springer, pp. 719–739, 2008.

[9] (2016, Apr.) [Online]. Available: http://www.piezo-tech.com/

[10] S. Johansson, O. Johansson, C. Mattsson, A. Jansson, and J. Eriksson, "Near-resonance electromechanical motor," U.S. Patent 6 747 394, 2004.

[11] S. Choi, and K. J. Kuchenbecker, "Vibrotactile display: Perception, technology, and applications," *Proc. IEEE*, vol. 101, no. 9, pp. 2093–2104, Sep. 2013.

[12] B. H. Choi, and H. R. Choi, "A semi-direct drive hand exoskeleton using ultrasonic motor," in *Proc. IEEE Int. Workshop Robot Human Interaction*, 1999, pp. 285–290.

[13] J. Maples, and J. J. Becke, "Experiments in force control of robotic manipulators," in *Proc. IEEE Int. Conf. Robot. Autom.*, 1986, vol. 3, pp. 695–702.

▷ **For more information on this or any other computing topic, please visit our Digital Library at** www.computer.org/publications/dlib.